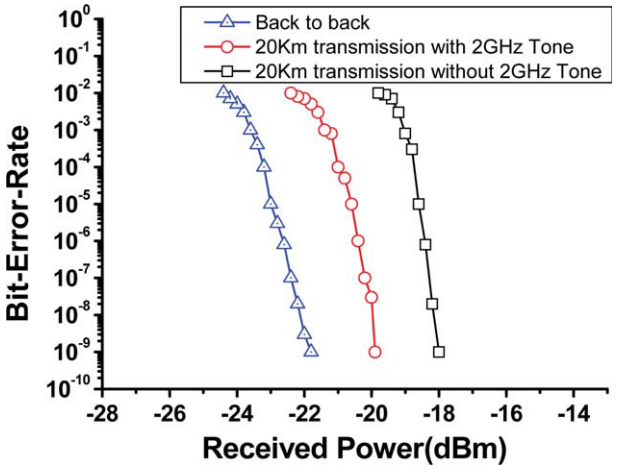

Figure 10 Upstream BER measurement at 1.25 Gb/s. [Color figure can be viewed in the online issue, which is available at wileyonlinelibrary.com]

4. CONCLUSION

We proposed a simple method of combining a RF tone in RSOA for reducing the Rayleigh backscattering induced degradation of upstream performance in a bidirectional optical link using the same wavelength. A combined RF tone generates increased frequency chirp, and it broadened the linewidth and reduced the effect of Rayleigh backscattering noise through effective noise spreading. A 2-dB power budget enhancement was achieved by this technique. This novel technique would be useful in application of WDM-PON using the same wavelength for both up/down link.

ACKNOWLEDGMENTS

This work was supported by the future technology laboratory of Korea Telecom (KT).

REFERENCES

1. R. Olshansky, V.A. Lanzisera, and P.M. Hill, Subcarrier multiplexed lightwave systems for broad-band distribution, J Lightwave Technol 7 (1989), 1329–1342.
2. R.D. Feldman, E.E. Harstead, S. Jiang, T.H. Wood, and M. Zirngibl, An evaluation of architectures incorporating wavelength division multiplexing for broad-band fiber access, J Lightwave Technol 16 (1998), 1546–1559.
3. J.-M. Kang and S.-K. Han, A novel hybrid WDM/SCM-PON sharing wavelength for up and down-link using reflective semiconductor optical amplifier, IEEE Photonics Technol Lett 18 (2006), 502–504.
4. S. Radic, N. Vukovic, S. Chandrasekhar, A. Velingker, and A. Srivastava, Forward error correction performance in the presence of Rayleigh-dominated transmission noise, IEEE Photonics Technol Lett 15 (2003), 326–328.
5. R.K. Staubli and P. Gysel, Crosstalk penalties due to coherent Rayleigh noise in bidirectional optical communication systems, J Lightwave Technol 9 (1991), 375–380.
6. D. Derickson, Fiber optic test and measurement, Prentice Hall, Upper Saddle River, 1998, Chap. 4, 5, 9.
7. P.K. Pepeljugoski and K.Y. Lau, Interferometric noise reduction in fiber-optic links by superposition of high-frequency modulation, J Lightwave Technol 10 (1992), 957–963.

SIMULTANEOUS MEASUREMENT OF THE DUAL-POLARIZATION PHASE VARIATIONS IN A MACH–ZEHNDER INTERFEROMETER

Ruey-Ching Twu,[1] Ming-Tsung Hsu,[1] and Yi-Fan Chu[2]
[1] Department of Electro-Optical Engineering, Southern Taiwan University, Tainan 710, Taiwan; Corresponding author: rctwu@mail.stut.edu.tw
[2] Institute of Nanotechnology, Southern Taiwan University, Tainan 710, Taiwan

Received 17 May 2010

ABSTRACT: *We propose a novel optical instrument to simultaneously measure the phase variations of both orthogonal linear polarizations in a Mach–Zehnder interferometer. An integrated Ti-indiffused $LiNbO_3$ Mach–Zehnder modulator is adopted for phase modulation and the optical homodyne scheme is used to measure the phase variations in the experimental setup. By using the multiplexed capabilities and flexible designs of a LABVIEW-based platform, the simultaneous measurements with real-time display of output interferomertic signals, spectrum results, and phase variations for both orthogonal polarizations, have been successfully demonstrated in this study.* © 2010 Wiley Periodicals, Inc. Microwave Opt Technol Lett 53:334–337, 2011; View this article online at wileyonlinelibrary.com. DOI 10.1002/mop.25703

Key words: *homodyne interferometry; Mach–Zehnder interferometer; phase measurement*

1. INTRODUCTION

The optical phase variations of a propagating light are dependent on the environments as well as the polarization states due to different boundary conditions. In optical metrology, the induced phase variations can be detected by using an optical interferometer. In a conventional Mach–Zehnder and Michelson interferometers, the input light splits into two different paths: one is as a reference path and another is as a sensing one. Then they combine again to produce an interferometric signal. Typically, a singly-polarized light is used, and the output intensity is dependent on a propagation phase difference between two paths. However, two orthogonally-polarized lights can also be used for measuring the polarization-dependent phase variations in the applications of surface plasmon resonance biosensors, phase-shifting interferometers, and interferometric ellipsometers [1–3]. Therefore, the simultaneous measurements of dual-polarization phase variations are essential in such measurement arrangements. Recently, the compact sensing modules have been studied extensively by using various integrated optical waveguide technologies [4–8]. The evanescent light propagation loss and phase variation are deeply dependent on the environmental conditions. By cladding layers onto the waveguides with different refractive indices will induce the changes of the effective refractive indices of the propagation modes in the waveguides [7, 8]. Therefore, the schemes of phase-sensitive measurements have been widely used in the past decade, although there are many options can be chosen to fabricate the passive waveguide transducers on different substrates. However, the sensing transducers integrated with optical phase modulations on the same substrates have more potential to improve the measurement dynamic range and precision [7–9].

In this study, a dual-polarization phase measurement system is proposed based on an optical homodyne technique. To evaluate the measurement performance of the proposed instrument, an integrated Ti-indiffused $LiNbO_3$ Mach–Zehnder modulator

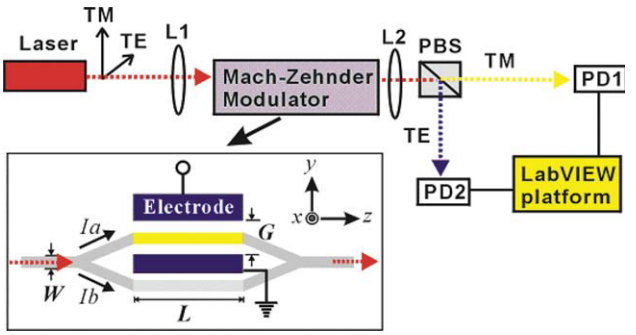

Figure 1 Measurement setup. [Color figure can be viewed in the online issue, which is available at wileyonlinelibrary.com]

fabricated in an *x*-cut/*z*-propagation substrate, is adopted to provide the optical phase modulations for the optical homodyne technique. The output interferometric signals are further characterized with spectrum analysis. The phase variations can be extracted by considering the related ratios between measured harmonic intensities [8]. A proof-of-concept experiment for simultaneous measurements on the dual-polarization phase variations is demonstrated by using simulated phase variations to test the measurement capabilities. Finally, the proposed LABVIEW-based (National Instruments) optical instrument has advantages of real-time and long-term monitoring for the measured data.

2. EXPERIMENTAL SETUP AND MEASUREMENT PRINCIPLE

Figure 1 shows a measurement setup of the proposed dual-polarization phase measurement system. A Ti-indiffused (TI) Mach–Zehnder modulator, fabricated in an *x*-cut/*z*-propagation $LiNbO_3$ substrate, is used to modulate the input phase signals of both transverse electric (TE) and transverse magnetic (TM) polarizations. A Ti-strip width of $W = 4$ μm and thickness of 33 nm was thermally indiffused at 1000°C for 4 h in a furnace with the oxygen ambient. The fabricated TI waveguide is single mode for both TE and TM polarizations. After the substrate end faces were polished, a silicon dioxide (SiO_2) buffer layer of 300 nm was deposited. Then 300 nm thick Aluminum electrodes were deposited and patterned by a standard photolithographic technique. The gap width G between parallel electrodes is 20 μm. The length of electrode L is 6 mm.

The light of a 633 nm He-Ne laser is launched into the waveguide via an objective lens $L1$ (40×). To excite TE and TM modes simultaneously, the incident linear polarization is oriented at 45° with respect to the *x*-axis of substrate. After passing through another objective lens $L2$ (40×) and a polarization beam splitter, the output beams of TE and TM polarizations were spatially separated into two paths. The received intensity signals from the two amplified photodetectors (PD1 and PD2) were sent to the LABVIEW platform for further analysis and real-time display of the measured data. The output intensities of the TE and TM polarizations (P_{TE} and P_{TM}) can be represented as

$$P_{TE,TM} = I_a + I_b + 2\sqrt{I_a I_b}\cos[\beta_{TE,TM}\sin(2\pi ft) + \phi_{TE,TM}(t)], \tag{1}$$

where I_a and I_b are the power intensities in the two splitting arms of the Mach–Zehnder modulator. The phase modulations of both TE and TM polarizations can be obtained by driving electric signals over the electrodes through electrooptic coefficients of r_{22} and r_{12} ($r_{22} = -r_{12}$, $r_{22} = 6.8$ pm/V). $\beta_{TE,TM}$ is the modulation depth defined as $\beta_{TE,TM} = \pi V_{ac}/V_\pi$, V_{ac} is the applied *ac* voltage, and V_π is the applied voltage for a π phase change. The notation of f is a modulation frequency. $\phi_{TE,TM}(t)$ is the time-varying phase difference between two arms. The received intensity signals are analyzed by the fast Fourier transform by using the LABVIEW-based software (version 8.5). The relations between different harmonic intensities (I_1, I_2, and I_3) and orders of Bessel functions (J_1, J_2, and J_3) are represented as follows:

$$I_1(f) = 4\sqrt{I_a I_b}\sin(\phi_{TE,TM})J_1(\beta_{TE,TM}), \tag{2}$$

$$I_2(2f) = 4\sqrt{I_a I_b}\cos(\phi_{TE,TM})J_2(\beta_{TE,TM}), \tag{3}$$

$$I_3(3f) = 4\sqrt{I_a I_b}\sin(\phi_{TE,TM})J_3(\beta_{TE,TM}). \tag{4}$$

The phase-difference variations of TE and TM polarizations can be extracted according to the related ratios between different harmonic intensities represented by

$$\phi_{TE,TM} = \tan^{-1}[I_1 \cdot J_2(\beta_{TE,TM})/I_2 \cdot J_1(\beta_{TE,TM})]. \tag{5}$$

To verify the capabilities of simultaneous measurements for both polarizations, a slow sinusoidal voltage V_{dc} at a frequency of 0.01 Hz was applied to accompany with the sinusoidal *ac* voltage of 10 V (peak-to-peak) at $f = 100$ Hz. The induced

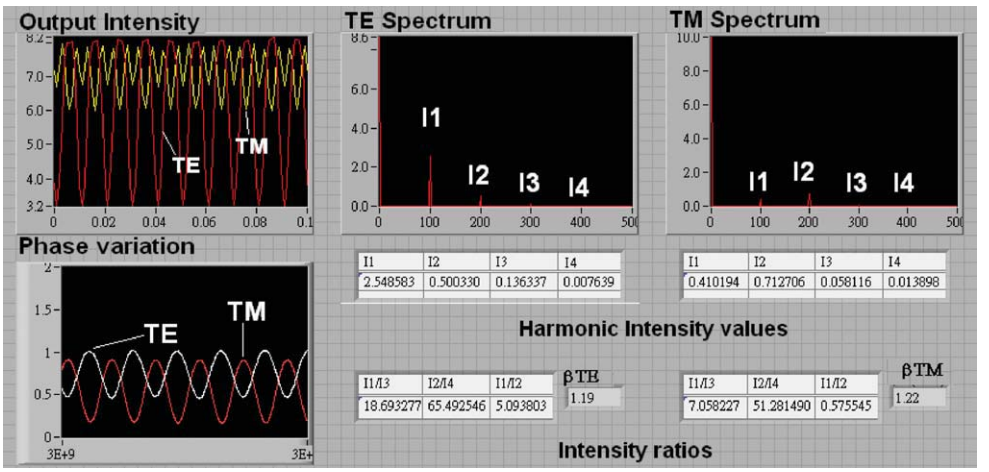

Figure 2 The LABVIEW front panel for simultaneously monitoring the measured data. [Color figure can be viewed in the online issue, which is available at wileyonlinelibrary.com]

electro-optic phase variations $\phi^{EO}_{TE,TM}(t)$ for the TE and TM polarizations can be represented by

$$\phi^{EO}_{TE,TM}(t) = (\pi/\lambda)Ln_o^3 r_{22,12}\Gamma_{TE,TM}(V_{dc}/G), \quad (6)$$

where λ is the wavelength of an input light, and n_o is the ordinary refractive index of the LN substrate ($n_o = 2.28$ at $\lambda = 633$ nm). Γ_{TE} and Γ_{TM} are the overlap integrals for the TE and TM polarizations, respectively.

3. RESULTS AND DISCUSSION

Figure 2 shows the designed LABVIEW front panel for monitoring the measured data, including output interferometric intensities, analyzed spectrums, harmonic intensities, intensity ratios, modulation-depth values, and calculated phase variations for both polarizations. The user-friendly panel provides advantages of easy manual control and real-time monitoring for related parameters. It is essential to optimize the input power to provide enough sensitivity to a photodetector and avoid a photorefractive effect of $LiNbO_3$ crystals. In this measurement, the maximum output intensities are 25 and 24 μW for the TE and TM polarizations, respectively. The phase-difference variations between two arms of the TI Mach–Zehnder modulator for both polarizations are shown in Figure 3. In the measurement period of 10 min, the means of the phase-difference variations are 0.72 and 0.54 rad for the TE and TM polarizations, respectively. The corresponding dynamic ranges of the phase-difference variations are 0.028 and 0.034 rad. The slight phase fluctuations can be observed due to the photorefractive effect in the TI waveguide, especially when they were irradiated with the laser at a 633 nm wavelength [10, 11]. The phase-stability observations can provide the evidence of acceptable input power level for developing the phase-sensitive $LiNbO_3$ waveguide sensors. To simulate the temporal phase changes for both TE and TM polarizations, a slow sinusoidal voltage at a frequency of 0.01 Hz, was applied to the same electrodes. The measured phase variations under different applied voltages are shown in Figure 4. The phase evolutions between the TE and TM polarizations have a π phase shift due to the opposite signs of r_{12} and r_{22} coefficients. In the case of $V_{dc} = 2$ V (peak-to-peak), Figure 4(a) shows that the dynamic ranges of phase changes are 0.23 and 0.29 rad for the TE and TM polarizations, respectively. According to Eq. (6), the calculated Γ_{TE} and Γ_{TM} are 0.465 and 0.587, respectively. As an increase of voltage up to $V_{dc} = 5$ V, Figure 4(b) shows that the dynamic ranges are 0.57 and 0.74 rad for the TE and TM polarizations, respectively. The calculated Γ_{TE} and Γ_{TM} are 0.461 and 0.598, respectively. The different overlap integrals of both polarizations are caused by the different boundary conditions for the orthogonally-polarized guided modes in the waveguides. These behaviors are also similar to the reported results [12]. We believe that the developed LABVIEW-based optical instrument shows advantages of real-time and long-term monitoring on the simultaneous measurements of the concerned parameters for both polarizations.

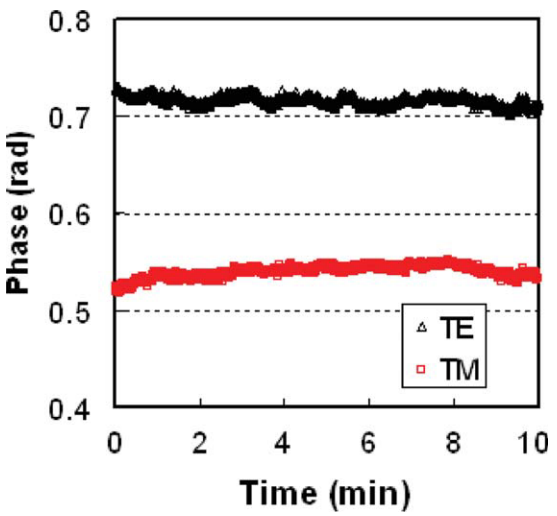

Figure 3 Phase variations versus time for both TE and TM polarizations. [Color figure can be viewed in the online issue, which is available at wileyonlinelibrary.com]

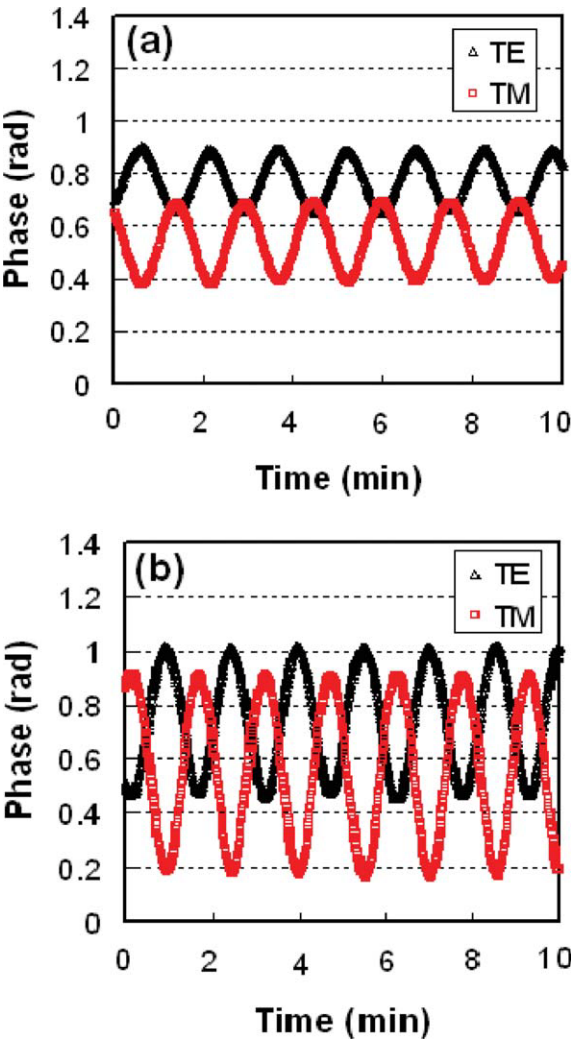

Figure 4 Phase variations versus time for both TE and TM polarizations under different applied voltages: (a) $V_{dc} = 2$ V and (b) $V_{dc} = 5$ V. [Color figure can be viewed in the online issue, which is available at wileyonlinelibrary.com]

4. CONCLUSION

In conclusion, we have successfully demonstrated a simple and a novel method for simultaneously measuring the phase-difference variations of a propagating light in a Mach–Zehnder interferometer when launching with both orthogonal linear polarizations. The research findings indicate that the proposed instrument is useful and has potential for the developments of a

phase-sensitive sensor integrated with a Mach–Zehnder modulator on the same $LiNbO_3$ substrate, in the near future.

ACKNOWLEDGMENTS

This work was supported in part by the National Science Council of Taiwan (NSCT), under Grant NSC 98-2221-E-218-006.

REFERENCES

1. S.Y. Wu, H.P. Ho, W.C. Law, and C. Lin, Highly sensitive differential phase-sensitive surface plasmon resonance biosensor based on the Mach–Zehnder configuration, Opt Lett 29 (2004), 2378–2380.
2. L.R. Watkins, Interferometric ellipsometer, Appl Opt 47 (2008), 2998–3001.
3. T. Kiire, S. Nakadate, and M. Shibuya, Phase-shifting interferometer based on changing the direction of linear polarization orthogonally, Appl Opt 47 (2008), 3784–3788.
4. S.H. Hsu and Y.T. Huang, A novel Mach–Zehnder interferometer based on dual-arrow structures for sensing applications, J Lightwave Technol 23 (2005), 4200–4206.
5. B.J. Luff, J.S. Wilkinson, J. Piehler, U. Hollenbach, J. Ingenhoff, and N. Fabricius, Integrated optical Mach–Zehnder biosensor, J Lightwave Technol 16 (1998), 583–592.
6. I. Suárez, R. Matesanz, I. Aguirre de Cárcer, P.L. Pernas, F. Jaque, R. Blasco, and G. Lifante, Antibody binding on $LiNbO_3$:Zn waveguides for biosensor applications, Sens Actuators B Chem 107 (2005), 88–92.
7. R.G. Heideman and P.V. Lambeck, Remote opto-chemical sensing with extreme sensitivity: design, fabrication and performance of a pigtailed integrated optical phase-modulated Mach–Zehnder interferometer system, Sens Actuators B Chem 61 (1999), 100–127.
8. B. Sepúlveda, G. Armelles, and L.M. Lechuga, Magneto-optical phase modulation in integrated Mach–Zehnder interferometer sensors, Sens Actuators A Phys 134 (2007), 339–347.
9. T.J. Wang and C.W. Hsieh, Surface plasmon resonance biosensor based on electro-optically modulated phase detection, Opt Lett 32 (2007), 2834–2836.
10. S. Thaniyavarn, Wavelength-independent, optical-damage-immune $LiNbO_3$ TE-TM mode converter, Opt Lett 11 (1986), 39–41.
11. N.A. Sanford and W.C. Robinson, Direct-current bias stable Ti:$LiNbO_3$ TE-TM mode converters produced by magnesium post-diffusion, Opt Lett 12 (1987), 531–533.
12. C.C. Chen, H. Porte, A. Carenco, Jean-Pierre Goedgebuer, and V. Armbruster, Phase correction by laser ablation of a polarization independent $LiNbO_3$ Mach–Zehnder modulator, IEEE Photonics Technol Lett 9 (1997), 1361–1363.

HIGH-FREQUENCY LOW-POWER LC DIVIDE-BY-2/3 INJECTION-LOCKED FREQUENCY DIVIDER

Y. N. Miao, C. C. Boon, M. A. Do, K. S. Yeo, and Y. X. Zhang
School of Electrical and Electronic Engineering, Nanyang Technological University, Nanyang Avenue, Singapore 639798, Singapore; Corresponding author: miao0012@e.ntu.edu.sg

Received 20 May 2010

ABSTRACT: *An LC divide-by-2/3 injection-locked frequency divider (ILFD) is described, where a pair of switched capacitors is used to select the division ratio between 2 and 3. The locking range analysis of the ILFD based on the gain and phase conditions is discussed. Based on the analysis, the optimized bias current in order to achieve the maximum locking range for the ILFD is obtained and is verified through measurement. The circuit was fabricated in a 0.18 μm CMOS technology. The input frequency of the divide-by-2/3 ILFD is from 4.28 to 4.81 GHz with an input power of −0.5 dBm. The power consumption of the ILFD is 3.15 mW at 1.8 V supply voltage.* © 2010 Wiley Periodicals, Inc. Microwave Opt Technol Lett 53:337–340, 2011; View this article online at wileyonlinelibrary.com. DOI 10.1002/mop.25694

Key words: *CMOS; divide-by-2; divide-by-3; injection-locked frequency divider (ILFD); LC-tank oscillator*

1. INTRODUCTION

Frequency dividers (FDs) take a periodic input signal and generate a periodic output signal at a fraction of the input frequency. They are widely used as an essential block of phase-locked loop (PLL) in frequency synthesizers and clock recovery systems. The output frequency of the PLL can be changed by the FD with variable division ratio in the feedback path. An LC injection-locked FD (ILFD) can achieve high frequency and low power but with a fixed division ratio, which is usually of 2 [1]. In Ref. 2, a divide-by-3 ILFD was proposed. In Ref. 3, an ILFD with multiple division ratio was proposed. However, the input frequencies for the divide-by-2 and divide-by-3 operations were different. Hence, it cannot be used as conventional divide-by-2/3 FD in a PLL.

In this letter, we present the design of an LC divide-by-2/3 ILFD, which has the same input frequency for the divide-by-2 and divide-by-3 operations. The ILFD operates at high frequency and consumes low power. In Section 2, the proposed circuit and its operation will be presented. In Section 3, the locking range will be analyzed based on the gain and phase conditions. In Section 4, the measurement results will be shown and discussed. In Section 5, the conclusions will be drawn.

2. DIVIDE-BY-2/3 FREQUENCY DIVIDER

The schematic of the proposed circuit is shown in Figure 1. The proposed ILFD consists of a differential ILFD and a pair of switched capacitors. The ILFD is based on an NMOS-type cross-coupled voltage-controlled oscillator with an injection transistor M_{inj}. The input of the ILFD is connected to the gate of M_{inj} while the drain and source of M_{inj} are connected to the differential output points V_{out+} and V_{out-}. The pair of switched capacitors is also connected to V_{out+} and V_{out-} as capacitive load. Each switched capacitor consists of a fixed capacitor C_a and an NMOS transistor M_a, which is switched on or off by a DC voltage V_{switch}. When V_{switch} is low, the switched capacitor

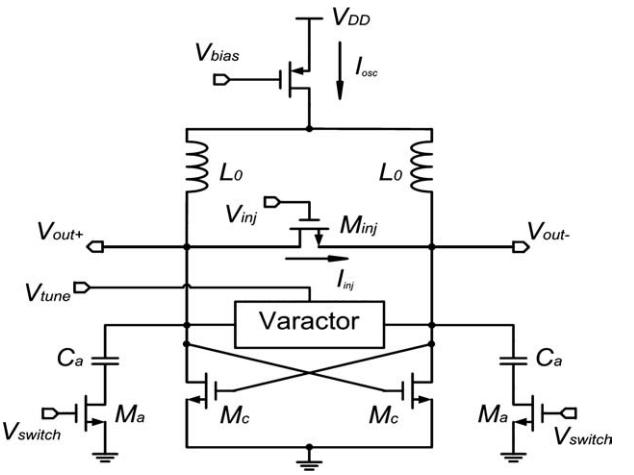

Figure 1 Schematic of the proposed divide-by-2/3 ILFD